



**Michigan
Technological
University**

Michigan Technological University
Digital Commons @ Michigan Tech

Department of Physics Publications

Department of Physics

1-15-2014

A technique to measure ice nuclei in the contact mode

Joseph Niehaus

Michigan Technological University

Kristopher W. Bunker

Michigan Technological University

Swarup China

Michigan Technological University

Alexander Kostinski

Michigan Technological University

Claudio Mazzoleni

Michigan Technological University

See next page for additional authors

Follow this and additional works at: <https://digitalcommons.mtu.edu/physics-fp>

 Part of the [Physics Commons](#)


Recommended Citation

Niehaus, J., Bunker, K. W., China, S., Kostinski, A., Mazzoleni, C., & Cantrell, W. (2014). A technique to measure ice nuclei in the contact mode. *Journal of Atmospheric and Oceanic Technology*, 36(3), 913-922.

<http://dx.doi.org/10.1175/JTECH-D-13-00156.1>

Retrieved from: <https://digitalcommons.mtu.edu/physics-fp/182>

Follow this and additional works at: <https://digitalcommons.mtu.edu/physics-fp>

 Part of the [Physics Commons](#)

Authors

Joseph Niehaus, Kristopher W. Bunker, Swarup China, Alexander Kostinski, Claudio Mazzoleni, and Will Cantrell

A Technique to Measure Ice Nuclei in the Contact Mode

JOSEPH NIEHAUS, KRISTOPHER W. BUNKER, SWARUP CHINA, ALEXANDER KOSTINSKI,
CLAUDIO MAZZOLENI, AND WILL CANTRELL

Michigan Technological University, Houghton, Michigan

(Manuscript received 11 July 2013, in final form 15 January 2014)

ABSTRACT

This study presents a new technique to study ice nucleation by aerosols in the contact mode. Contact freezing depends upon the interaction of a supercooled droplet of water and an aerosol particle, with the caveat that the particle must be at the air–water interface. To measure nucleation catalyzed in this mode, the technique employs water droplets that are supercooled via a temperature-controlled copper stage, then pulls aerosol-laden air past them. Particles deposit out of the airstream and come into contact with the surface of the droplet. The probability that a particle–droplet collision initiates a freezing event, necessitating knowledge of the total number of particles that collide with the droplet, is reported. In tests of the technique, ice nucleation by the bacteria *Pseudomonas syringae* is found to be more efficient in the contact mode than in the immersion mode by two orders of magnitude at -3°C with the difference diminishing by -8°C .

1. Introduction

Atmospheric aerosol may catalyze the formation of ice in Earth's atmosphere through four known nucleation pathways or modes—deposition, immersion, condensation, and contact. In deposition mode nucleation, water vapor adsorbs to the aerosol particle and forms ice directly, without an intervening liquid stage. Immersion and condensation mode nucleation require the presence of the bulk supercooled liquid; the difference between the two is primarily in how the particle comes to be surrounded by the liquid phase. In contrast to the first three, contact mode nucleation is initiated by a supercooled droplet of water coming into contact with an aerosol particle. It is the presence of the particle at the air–water interface that triggers the freezing event.

The deposition, immersion, and condensation modes may be quantified by exposing aerosol particles to the appropriate combinations of relative humidity and temperature. For example, deposition nuclei (i.e., those aerosol particles that are active as ice nuclei in the deposition mode at a given temperature) can be detected and counted by exposing aerosol particles to a known temperature and relative humidity with respect to ice. Ice

crystals are then the result of deposition nucleation, since the probability of homogeneous nucleation of ice directly from the vapor phase is vanishingly small. The immersion and condensation modes can be quantified by first exposing the aerosol to a supersaturation with respect to water and then exposing the subsequent droplet to a low temperature and monitoring its phase.

Numerous methods have been employed over the past 50 years to accomplish such processing, including filter samples (see, e.g., Roberts and Hallett 1968; Bundke et al. 2008), mixing chambers (e.g., López and Ávila 2013), and parallel plate diffusion chambers (e.g., Rogers 1988; Hussain and Saunders 1984; Tomlinson and Fukuta 1985). The key element in all of the instruments is that an aerosol particle's ice nucleation activity is indicated by the presence or absence of ice crystals after all of the particles have been exposed to some combination of temperature and relative humidity.

Measurements of contact nucleation, unlike deposition and immersion/condensation, cannot be done only by exposing the aerosol to combinations of relative humidity and temperature because aerosol particles must be at the supercooled water droplet's surface. Liquid water and aerosol interactions must be quantified as well as any subsequent freezing event. Initial observations of the phenomenon were carried out by sprinkling powders onto supercooled droplets that were supported on a substrate (Gokhale and Gooled 1968), or by placing the powder next to the droplet and gently

Corresponding author address: Will Cantrell, Dept. of Physics,
Michigan Technological University, 1400 Townsend Dr., Houghton,
MI 49931.
E-mail: cantrell@mtu.edu

nudging the powder until it made contact (Fletcher 1972). Since then, techniques to measure contact nucleation have included cold plates (Fornea et al. 2009; Shaw et al. 2005), droplets suspended in electrodynamic traps and wind tunnels (Hoffmann et al. 2013; Svensson et al. 2009; Pitter and Pruppacher 1973), and flow-through cloud chambers (Ladino et al. 2011). [For a more comprehensive review of the techniques and instruments that have been used to measure contact nucleation, see Ladino et al. (2013).]

In some configurations (e.g., those used by Fletcher 1972; Shaw et al. 2005; Fornea et al. 2009), cold plates have the advantage of minimizing the uncertainty in the number of particle–droplet contacts that have occurred, because the contact between nucleating agent and supercooled droplet is physically observed. For heterogeneous ice nucleation, the main catalyst of freezing is particle–droplet interactions, and these instruments provide for very controlled environments. The disadvantage in those cases is that the contact area between particle(s) and droplet is relatively large, far greater than the typical aerosol particle–droplet interaction in the atmosphere. Hence, collision rates and the number of collected particles may not be indicative of atmospheric conditions. This condition could, however, be a boon in that much larger number concentrations can be probed to provide information about the nucleation process itself. Cold plates are also typically restricted to temperatures greater than about -25°C because larger droplets, which have a large contact area with the supporting substrate, usually freeze at $T < -25^{\circ}\text{C}$ simply because of the contact with the substrate. (Larger droplets do not bias the contact nucleation itself because the radius of curvature, which is the primary difference between droplets and bulk water, of even $10\text{-}\mu\text{m}$ -diameter droplets is large enough to have little effect on the molecular-scale interaction between the aerosol particle and the droplet.) The final restriction is that cold plates are usually more labor intensive, since droplets must be replaced once they are frozen.

Electrodynamic traps (Hoffmann et al. 2013; Svensson et al. 2009), wind tunnels (Pitter and Pruppacher 1973), and flow-through cloud chambers (Ladino et al. 2011) can access much lower temperatures (the homogeneous nucleation limit) because the droplet is suspended in air. Such systems can usually process a larger number of droplets, which improves the statistics in terms of the number of freezing events observed. However, an increase in the number of observed freezing events usually comes at the expense of fewer aerosol–droplet interactions. The systems are also limited to lower temperatures because of the range of droplet sizes that can be levitated; for higher temperatures smaller droplets evaporate quickly and collide with no (or not enough)

particles. Determination of the number of aerosol particle–droplet interactions is also more difficult in such systems (Svensson et al. 2009; Ladino et al. 2011). Hoffmann et al. (2013) address this issue by both a calculation and an empirical measure of particles in the droplet via a scanning electron microscope (SEM). They calibrate their system and equation for known flow velocity, aerosol size, droplet charge, and aerosol volume flow. Our approach is similar in that it is specific to the constraints of our instrument design, but we require no flow calculations of aerosols in air.

We have developed a technique to measure the efficiency with which aerosol particles catalyze freezing in the contact mode for temperatures greater than approximately -24°C , where contact freezing is expected to be the dominant mechanism of freezing for nonbiological particles. We employ test droplets supported on a cold stage with the aerosol sample in the airstream that is pulled past the test droplet. Our system combines features of the approaches outlined above, which allows us to expose test droplets to aerosol particles of atmospherically relevant sizes and to reliably estimate the number of particles that are deposited to the test droplet before a freezing event.

2. Overview

The goal of the experiment is to measure the nucleating efficiency of a sample aerosol in the contact mode as a function of temperature. We define the efficiency as

$$E = \frac{F}{N_d}, \quad (1)$$

where F is the total number of freezing events and N_d is the sum of particles on or in the droplets. (We assume that aerosol particles do not bounce off the liquid water surface.) Efficiency E can be interpreted as answering the question, “What fraction of the aerosol particles that come into contact with the surface of the droplet result in a freezing event?” An efficiency of 10^{-3} means that 1000 particles were deposited to the surface of the droplet before freezing occurred.

In our experiments, to measure the nucleating efficiency, a water droplet is cooled to the desired temperature and exposed to a flow of aerosol until it either freezes or the testing time has expired. The maximum length of the tests is taken so that the droplets’ size and shape are not significantly altered by evaporation. The system was flushed with dry, filtered air to eliminate the possibility of contamination in each test before aerosol was introduced to the system.

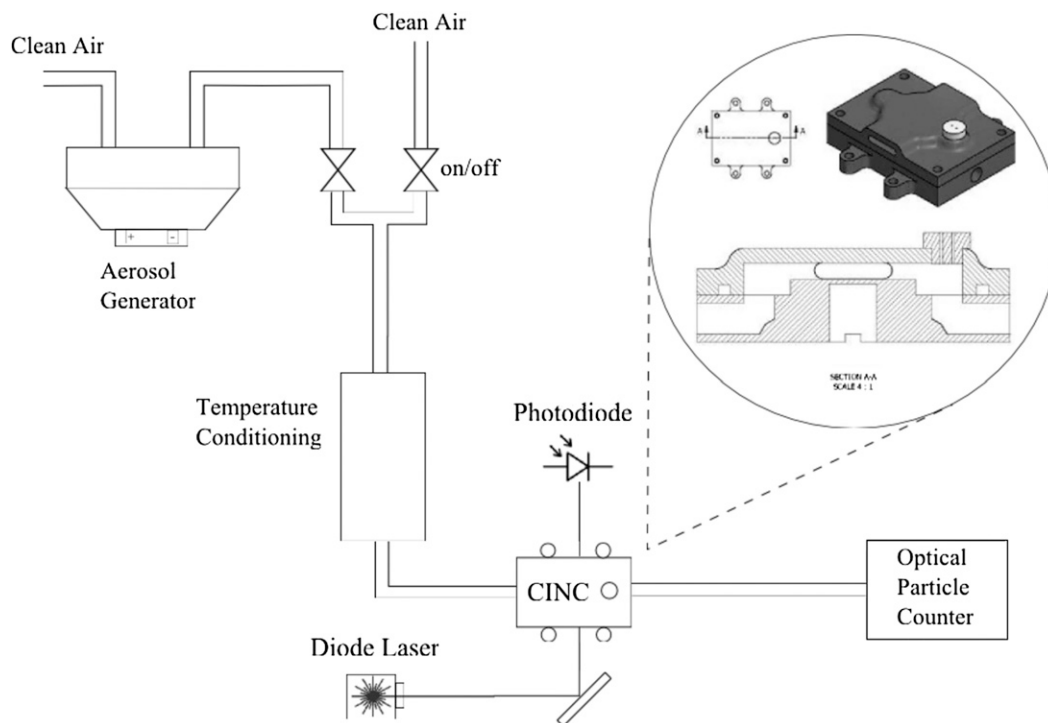


FIG. 1. Schematic of the experimental design. The CINC is shown in the inset. A more detailed cross section is shown in Fig. 2.

The experiment consists of four major components. In procedural order, they are aerosol generation, conditioning of the air and aerosol stream, monitoring of the phase of the test droplet, and counting the aerosol particles that exit the nucleation chamber. A schematic of the design is shown in Fig. 1. For our laboratory tests, air enters the system from a dry high-efficiency particulate absorption (HEPA)-filtered source into the aerosol generator. The sample stream is then processed through temperature conditioning. The flow passes through the ice nucleation chamber and exits through an aerosol particle counter. The two valves before the air conditioner allow for easy switching between clean air and aerosol. A water droplet inside the contact ice nucleation chamber (CINC) sits in the path of the airflow; a small fraction of the aerosol particles in the flow is deposited to it. Upon freezing, light from a laser focused through the droplet scatters, and the corresponding drop in signal from the photodiode is observed. Linear polarizers may also be placed in the path of the beam with one before and one after the CINC to allow phase monitoring via repolarization of the laser beam. Water does not polarize light and thus polarizers set 90° from each other will completely block the beam, while ice will repolarize the light and the photodiode will register a signal. This system allows us to monitor the phase of a water droplet in the

presence of aerosol flow. The number of particle–droplet interactions is calculated by the two methods described in section 4.

3. Ice nucleation stage

The heart of the technique is CINC, which is designed to support the test droplet at a specified temperature and to allow monitoring of the phase of the droplet as the stream of test aerosol flows past it. The CINC is a milled copper stage; a cross section is shown in Fig. 2. Windows cut through the side of the top plate allow monitoring of the phase of the $5 \pm 0.1 \mu\text{L}$ test droplet, which sits on a silanized glass slide (Hampton Research, HR3–231) placed on the center stage of the bottom piece.

Freezing events in the chamber are detected by focusing a 1-mW 650-nm diode laser through the droplet to a photodiode on the other side. When a freezing event occurs, the beam is scattered and the photodiode voltage drops to zero. For higher temperatures, the ice that forms is clearer and only a minor dip in signal is observed. After every test, the top is removed and the droplet is physically inspected, resulting in zero uncertainty for F , the number of freezing events. When in situ immersion control tests were performed, the top was not removed and instead the freezing event was confirmed by a very distinct signal

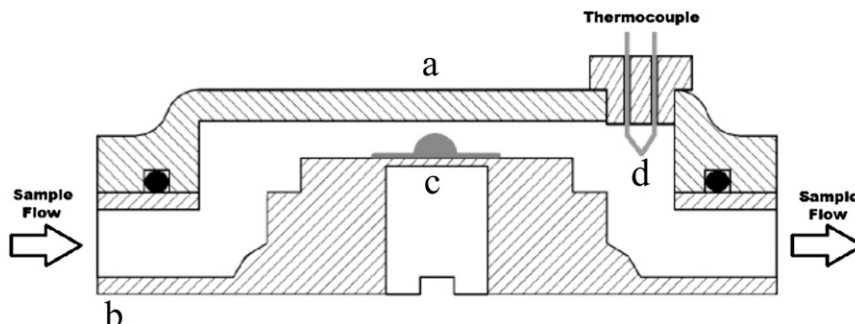


FIG. 2. Cross section of the CINC with letters denoting points where temperature is measured. Platinum RTDs are used at points A–C. A K-type thermocouple is used at point D. The path of the diode laser beam is into the page.

drop in the photodiode and accompanying temperature change in the thermocouple downwind of the droplet.

The other relevant parameter in the determination of E is the number of particles that deposit to the droplet, which is, in turn, determined by the characteristics of airflow in the chamber. The volumetric flow rate for our experiments is chosen to be 1 liter per minute (L min^{-1}), giving a linear flow velocity of about 0.7 m s^{-1} at the 1/4-in. inlet to the chamber. The Reynolds number for the flow of air past the hemispherical water droplet is approximately 200, which indicates that the flow is in an intermediate regime between turbulent and laminar. The flow in the chamber precludes a simple calculation of the number of particles deposited to the test droplet; we use an empirical method instead, described in section 4.

Aerosol particles that exit the CINC are counted with an optical particle sizer (OPS; TSI model 3330). It measures the number and size of particles by collimating the flow and recording light scattered by each particle. With dead time corrections, the OPS is accurate to approximately $\pm 10\%$ of the total number. Alternatively, a TSI condensation particle counter (model 3772) is available. It provides a more accurate reading for number concentrations but contains no information about the size of the particles.

Finally, the temperature of a test droplet in the CINC can be selected by an Accuthermo FTC100D thermoelectric cooler (TEC) temperature controller coupled with a 12.25-cm^2 square Ferrotec thermoelectric Peltier element. The controller and Peltier element have a heat pumping capability of 30 W, enough to cool the chamber at a rate of $\sim 5^\circ\text{C min}^{-1}$. The hot side of the element is cooled by a copper heat sink through which ethylene glycol circulates. The coolant is pumped by a Julabo CF40 Cryo-Compact Circulator; the temperature of the coolant is set to -20°C . Temperatures of 30° to -30°C are possible, though the practical, lower limit of the chamber is $-23.5 \pm 0.2^\circ\text{C}$, which is set by the heterogeneous freezing limit of test droplets on the glass slides.

The temperature sensor for the FTC100D TEC's control loop is a thin film, three-wire 100Ω platinum resistance temperature detector (RTD; Minco); it is located in the recess indicated as point C in Fig. 2. Two four-wire RTDs of the same type monitor temperatures at points A and B. A K-type thermocouple (Omega) 1/16-in. thick protrudes into the airstream at point D.

As noted above, the temperature of the test droplet is not controlled directly. The RTD in the Accuthermo's control loop is approximately 0.5 mm below the droplet. The thickness of the copper stage is 0.5 mm at that point, and the glass slides are ~ 0.03 mm thick. To determine the temperature of a test droplet for a given setting of the temperature controller, we calibrated the stage using the melting point of the four substances summarized in Table 1. Droplets of the alkanes or water on the CINC stage were cooled until they froze. The frozen droplets were then warmed slowly until melting was observed with a charge-coupled device (CCD) camera. A modified chamber top with a window allowed for a clear view of the stage and samples. Close to the melting point, the temperature, as read by the RTD at point C, was increased by 0.1°C steps. The droplet was observed at the new temperature for at least 300 s, adequate time for the latent heat of melting to be transferred to the sample. If melting was not observed, then the temperature was increased by

TABLE 1. Substances used to calibrate the temperature of a droplet on the CINC stage. The measured temperatures are those from the RTD at point C in Fig. 2, while the melting point values of the decanes are taken from Finke et al. (1954).

Sample	Melting point ($^\circ\text{C}$)	Temp at point C ($^\circ\text{C}$)
n-undecane	-25.56	-24.85
n-dodecane	-9.56	-9.55
Pure water	0	-0.85
n-tetradecane	5.88	4.75

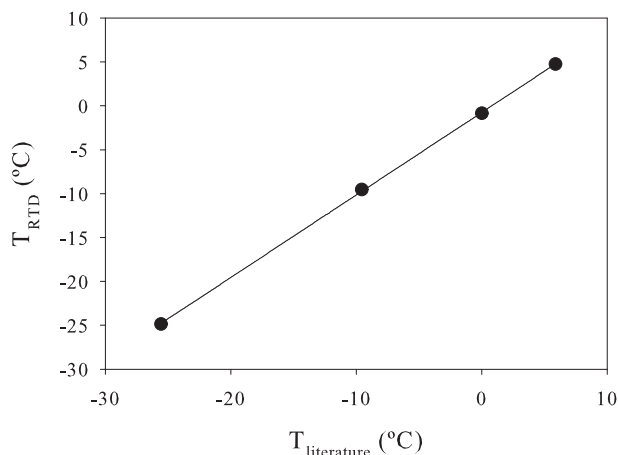


FIG. 3. Reading of the RTD located at point C in the CINC (see Fig. 2) as a function of the melting point temperature of selected alkanes and water. The linear regression used to determine other temperatures is shown.

another 0.1°C and the procedure repeated. The readings of the RTD at point C when the sample droplet melted are shown in the final column of Table 1. Melting was never observed at a temperature lower than what is indicated in the table. In other words, a droplet of pure water does not melt on the stage in the CINC for a temperature reading of 272.2 K , but it melts within 30 s once the temperature at point C is increased to 272.3 K . Results shown in Table 1 are from tests conducted in still air. Selected tests were repeated with air flowing through the system, and no change in T_m was observed. This is expected because the heat flux is dominated by contributions from the bottom plate; the heat flux from air is negligible.

Figure 3 is a plot of the RTD reading at point C in the chamber as a function of the melting point of the substance on the CINC stage. We interpolate to other temperatures using a linear regression, also shown in Fig. 3. Combining the results from Table 1 and the residuals of the fit shown in Fig. 3, we conclude that the uncertainty in the temperature of a test droplet on the CINC stage is $\pm 0.2^{\circ}\text{C}$.

4. Determining the number of aerosol–droplet interactions

Controlled studies of contact mode nucleation are difficult because the aerosol particles that trigger freezing are commonly too small to be observed or tracked. Our approach is to obtain a statistical measure for the number of particles that deposit to the droplet. We present this number as the collected fraction, defined as

$$\text{CF} = \frac{N_d}{N_C}, \quad (2)$$

where N_d is the number of aerosol particles that have been deposited to the droplet's surface and N_C is the number of particles counted by the particle counter at the exit to the CINC (see Fig. 1). It should be noted that the CF is constant with respect to time and directly measures the ratio of surviving particles counted by the OPS and those found inside the droplet. Hence, deposition of aerosol particles to other parts of the chamber or air lines are accounted for. The uncertainties derived include variations in droplet placement, air densities, particle sizes, and flow geometries. The CF is strictly a statistical measure of our deposition rate of aerosol particles in terms of the number counted at the end of the system.

In the denominator of Eq. (1), N_d is the quantity of interest. It is not feasible to count particles inside every test droplet after every nucleation test; instead, we determine CF in separate experiments, described below, then measure N_C and use Eq. (2) to find the number of particles deposited to a droplet in a particular test. The value of CF that we use is for flow conditions in the CINC at 1 L min^{-1} , and these conditions are never altered during subsequent experiments.

a. Method 1

Kaolinite particles were size selected with a differential mobility analyzer (DMA; TSI 3081) and pulled past water droplets in the CINC; to facilitate analysis with an SEM, test droplets were placed on carbon tape on a glass slide. The number of aerosol particles exiting the chamber was counted with the condensation particle counter (TSI, model 3772). The airflow was then turned off, the droplets were allowed to evaporate, and the carbon tape was transferred to an Al stub for analysis.

The residue shown in Fig. 4 was imaged using an SEM. Individual particle counts cannot be readily determined because particles agglomerate during evaporation and become indistinguishable from each other (see, e.g., Fig. 5).

Instead, the number of particles which collided with the test droplet ($N_{d,1}$) is estimated as

$$N_{d,1} = \frac{A_r}{\bar{A}_p}, \quad (3)$$

where A_r is the total surface area of the residue obscured by dust and \bar{A}_p is the average cross-sectional size of a particle for the size selected by the DMA. The cross-sectional area was determined in separate experiments

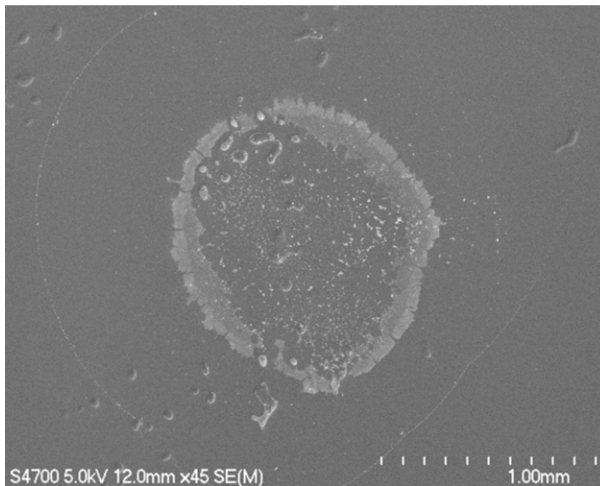


FIG. 4. Residue of kaolinite particles after a test droplet in the CINC evaporates.

by, for example, selecting a mobility diameter (D_m) of 500 nm and examining many single-particle cross sections on the filter substrate with the SEM. The mean area of a single particle was found to be 1.1 ± 0.1 and $1.9 \pm 0.2 \mu\text{m}^2$ for 1- and 0.5- μm mobility diameter size selections, respectively.¹

Results are shown in Table 2. The uncertainty in the number of particles deposited to the droplet is derived from the uncertainty in the projected area of one particle, stated above, and the uncertainty in A_r , the total projected area of the dust in the residue of the evaporated droplet, which we conservatively estimate is 25%. The estimation comes from uncertainties in determining surface area of irregularly shaped particles. As the residue evaporates, the kaolinite will agglomerate, fusing into larger masses, making single-particle identification difficult. Furthermore, medium-resolution images were required to capture pictures of the entire residue in a timely fashion. The uncertainty is derived from difficulties in distinguishing between single particles and the

¹The apparent reversal in the average surface areas for the 0.5- and 1- μm -diameter particles stems from the fact that the DMA selects the particles' mobility diameter, which is inherently three dimensional, since it relies on a drag force balancing the electric force exerted on the charged particle. The DMA is selecting the correct mobility, verified with polystyrene latex spheres. However, kaolinite is not spherical—it is flaky. The area we see in an SEM image is consistent with a 1- μm diameter, but the thickness is only 100 nm or so. We have verified this in a couple of cases using a tilted SEM stage (the 500-nm particles seem to be flakier than the 1 μm). We are pursuing this issue further by analyzing the dust using an atomic force microscope, which gives us the three-dimensional image of the particles, not just their 2D projection. That, however, is beyond the scope of this paper.

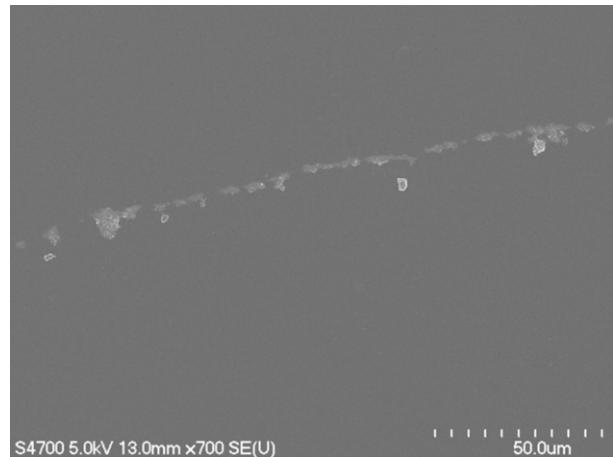


FIG. 5. Edge of the residue that shows a couple of obvious individual particles; most of the rest of the edge are particles that have agglomerated as the droplet evaporated.

challenge of strictly bounding particle residues from SEM images.

b. Method 2

As a check on the collected fractions just described, we used spherical glass beads 5.4 μm in diameter (Thermo Scientific, Duke Standards 9000 Series) instead of size-selected dust. Even though the glass beads also clump together as the droplet evaporates, their uniform size and shape enables an accurate count of the individual particles within the residue of an evaporated droplet, using a 1000 \times optical microscope. The results are summarized in Table 3.

c. Comparison of the methods

A comparison of the data in Tables 2 and 3 shows that, for our experimental setup, the collected fraction is not a strong function of the size of the aerosol particle for particles larger than 1 μm in diameter, as the kaolinite and glass beads were deposited to the test droplets with the same efficiency and almost the same variability. For every thousand particles in the size range 1–5 μm that go through the CINC (i.e., are counted by the OPS), between three and nine particles are deposited to the droplet, with a mean of six.

The uncertainty in the efficiency of contact ice nuclei in our experiments is dominated by the intrinsic variability in the number of particles that collide with the test droplet for any given experiment. The uncertainty in E is given by

$$\sigma_E = \frac{F}{N_d^2} \sqrt{\sigma_{N_c}^2 CF^2 + \sigma_{CF}^2 N_c^2}, \quad (4)$$

TABLE 2. Data from tests used to determine the collected fraction of kaolinite. The average projected area of a single particle of the size selected dust is denoted by $A_{1\text{particle}}$.

D_m (μm)	Test No.	$\overline{A}_{1\text{particle}}$ (μm^2)	$N_{d,1}$	N_C	CF
1.0	1	1.1 ± 0.1	4000 ± 1000	566 125	$7 \times 10^{-3} \pm 2 \times 10^{-3}$
	2		2000 ± 500	357 203	$6 \times 10^{-3} \pm 2 \times 10^{-3}$
0.5	1	1.9 ± 0.2	1700 ± 500	2 141 805	$8 \times 10^{-4} \pm 2 \times 10^{-4}$
	2		700 ± 200	477 059	$16 \times 10^{-4} \pm 2 \times 10^{-4}$

which shows that the uncertainty is inversely proportional to the square of the number of particles deposited to the droplet. The variation in the collected fraction is the principal contributor to the total uncertainty.

5. Measurements

Nucleation tests were performed with the bacteria *Pseudomonas syringae*, which has a well-characterized immersion mode freezing behavior (see, e.g., Maki et al. 1974). The dust sample was generated by grinding pellets of Snomax (Snomax International), which is a dried form of the bacteria, and then dispersing the resulting powder with a custom-built vibrating membrane dust dispersal system (see the appendix). A representative size distribution of the aerosol, taken just after the sample stream has exited the CINC, is shown in Fig. 6. We note that for tests run at $T > -5.0^\circ\text{C}$, crossed polarizers were used to detect the onset of ice formation due to the more transparent nature of the solid formed.

The contact freezing efficiency of the aerosolized Snomax, defined by Eq. (1), is plotted as a function of temperature in Fig. 7. For the tests reported here, we use $\text{CF} = 5 \times 10^{-3} \pm 3 \times 10^{-3}$, which is the mean of the collected fractions reported in sections 4a and 4b above. The uncertainty is the standard error of the mean. Like the immersion mode, the efficiency is low for the higher temperatures and has an asymptotic approach to 10^{-1} at -8°C . No freezing events were observed for temperatures

TABLE 3. Results of tests to determine the CF, using glass beads of $5.4 \mu\text{m}$ in diameter. The mean collected fraction is 0.006 ± 0.003 .

N_C	$N_{d,2}$	CF
4054	34	0.0084
4324	24	0.0056
5125	8	0.0016
5869	29	0.0049
6239	45	0.0072
7867	35	0.0044
8605	94	0.0109
8801	46	0.0052
9454	37	0.0039
9960	74	0.0074

greater than -3°C ; based on our experiments, the efficiency of Snomax in the contact mode is less than 10^{-6} for $T > -3^\circ\text{C}$.

The asymptotic approach to $E = 10^{-1}$ instead of 1 is a bit puzzling at first. However, there is evidence suggesting that not every *P. syringae* cell expresses the protein that catalyzes the formation of ice at high temperatures. A recent study of ice nucleation of Snomax in the immersion mode showed that even at -30°C , only 20%–30% of droplets containing a 650- or 800-nm Snomax particle froze (Hartmann et al. 2013), which is consistent with our results.

One benefit of using bacteria is that the number of cells can be calculated from the size of the particles. *P. syringae* cells are rod shaped and have a known size of $\sim 2.0 \mu\text{m}$ long and $1 \mu\text{m}$ in diameter (Monier and Lindow 2003). From the size information measured by the OPS, we can calculate the number of cells that collide with the droplet and compare this directly with immersion mode freezing.

6. Distinguishing contact mode

Inevitably, particles that deposit to the water surface end up in the interior of the droplet and may contribute to

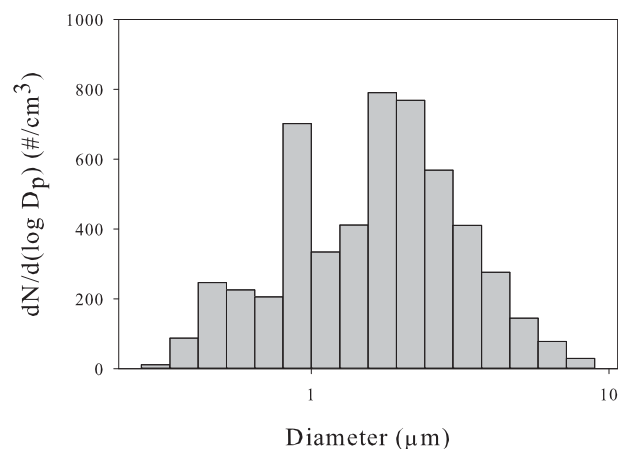


FIG. 6. Average size distribution of Snomax measured by the OPS, immediately after the CINC. Uncertainties are given by the manufacturer (TSI) of 10% of the number concentration in any size bin.

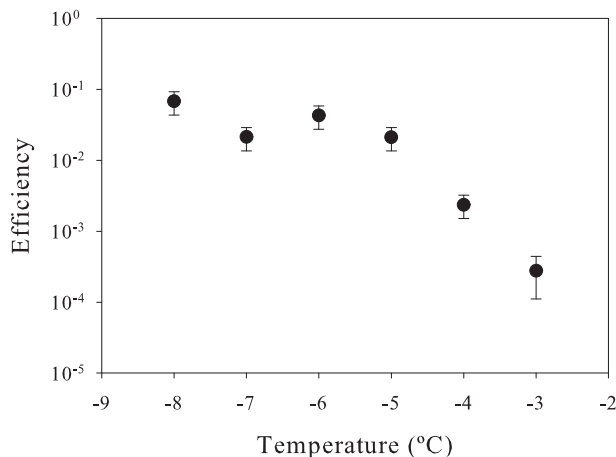


FIG. 7. Efficiency of Snomax particles measured by the CINC.

immersion mode freezing. Airflow over the surface of the test droplet causes circulation eddies that pull particles inside and mix them. To distinguish our contact freezing events from those that may have been caused from particles inside the droplet, two measures were taken.

First, many droplets that presumably froze in the contact mode were warmed to 10°C. They were then cooled back to the same temperature at which the test was performed and held steady with clean airflow for 30 min. No freezing events occurred. Furthermore, it was found that the droplets that froze at -3°C from Snomax could be supercooled below -8°C before they would spontaneously freeze.

Using diameters reported by the OPS, the number of bacterial cells in an aerosol particle can be calculated. For this analysis, particles smaller than $1\ \mu\text{m}$ were ignored because they are most likely nutrient media from the sample preparation. Particles from the sizes 1 to $2.5\ \mu\text{m}$ were taken to have only one cell, and larger particles had the equivalent spherical volume divided by the volume of a bacterial cell to determine the number of cells. The results were plotted along with immersion mode data from Maki et al. (1974) in Fig. 8. Maki et al. (1974) executed a series of immersion ice nucleation tests on a cultured form of *P. syringae* strain C-9. They did so by preparing a series of droplet freezing assays and measuring the number of droplets frozen and the temperature. The data represent the temperature at which 50% of the droplets froze, and the temperature range is given between the onset temperature and T_{99} , where 99% of the droplets froze. The plot shows that from our tests, the contact mode of Snomax is significantly more effective than immersion mode for all temperatures measured. This difference diminishes as the temperature decreases. Through these two pieces of evidence, we conclude that none of the freezing events that we observed in our experiments was due to immersion nucleation.

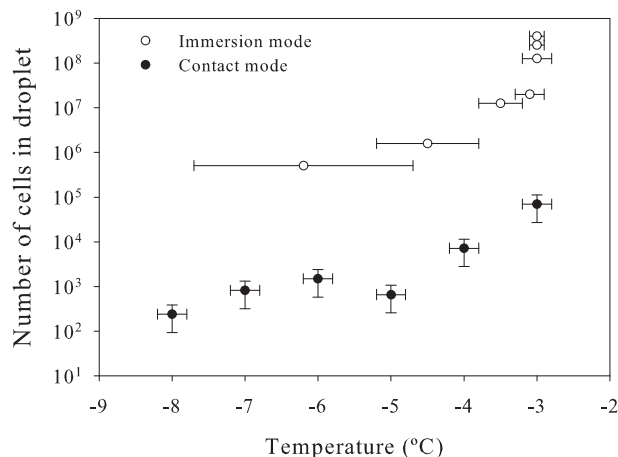


FIG. 8. Open circles are immersion freezing tests adapted from Maki et al. (1974), and filled circles are contact freezing tests from above. Maki et al. report T_{50} , the temperature at which 50% of the droplets in their freezing assay turned to ice. The bounds on their data are the temperatures at which the droplets started freezing (onset T) and T_{99} , the temperature at which 99% of their droplets froze. Contact mode for Snomax appears to be more active for all temperatures, but both modes are expected to converge for colder temperatures.

7. Concluding remarks

We have developed a technique to measure the efficiency with which aerosol particles catalyze freezing in the contact mode for temperatures greater than approximately -24°C , a range that is relevant for tropospheric, mixed-phase clouds. Measurement of contact freezing requires that aerosol particles come into contact with the surface of supercooled droplets of water, and that the resulting freezing event (if there is one) be detected. We accomplish that by using test droplets supported on a cold stage; aerosol particles deposit to the droplet from the airstream flowing through our contact ice nucleation chamber (CINC). We monitor the phase of the test droplet with a diode laser and photodiode, and determine the number of particles that have hit the droplet by examining the evaporated residue of test droplets in separate experiments. Our technique combines elements of traditional cold stage measurements with aspects of flow-through cloud chamber or electrodynamic trap techniques, which allows us to access the temperature range of approximately -24°C to 0° and nucleation efficiencies of 10^{-6} to 1.

The temperature range of the system is currently limited by the temperature at which pure water droplets on the silanized glass slides freeze (approximately -25°C). We are exploring methods to suspend relatively large droplets ($\sim 1\ \text{mm}$) in an acoustic levitator to circumvent this, though we note that the determination of E is even more difficult in that case than what we have described here. To alleviate that difficulty, we are attempting to

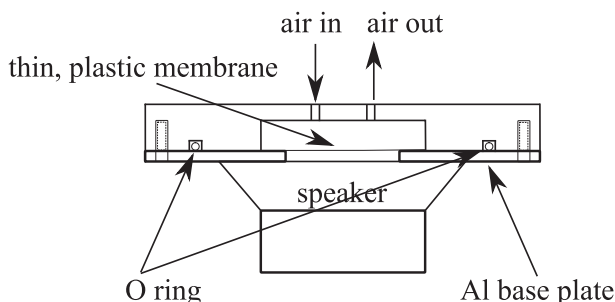


FIG. A1. Schematic of the dust dispersal system. The speaker drives oscillations in the thin membrane; the vibrating membrane lofts the aerosol particles into the airstream.

develop optical methods that will enable detection of single-aerosol particle–droplet collisions. The size of the aerosol particles that we can test using our technique is also limited. Anything larger than about $10\text{-}\mu\text{m}$ diameter settles or impacts out. (Our tests show that we lose a lot of the $10\text{-}\mu\text{m}$ particles before they reach the CINC.) Orienting the flow path in the vertical will solve most of those problems; such a modification is being designed.

The technique we have developed to quantify the efficiency with which aerosol particles in the size range $0.3\ \mu\text{m} < D_p < 10\ \mu\text{m}$ catalyze freezing in the contact mode will improve our understanding of ice processes in mixed-phase clouds. For example, we are currently evaluating contact freezing efficiencies for mineral dusts of atmospheric relevance. Currently, most cloud models do not include parameterizations of contact freezing, which are well constrained by measurements (Yun and Penner 2012). Laboratory data such as what we have shown here will narrow the uncertainties associated with ice processes. Additionally, our technique could be adapted for use in the field, though an aerosol concentrator would probably be necessary in that case to improve the signal-to-noise ratio.

Acknowledgments. This work was funded through the National Science Foundation Grants AGS-1028998, AGS-1039742, and AGS-1119164. Swarup China acknowledges a NASA Earth and Space Science Graduate Fellowship. Ashima Chhabra, who was funded through the Michigan University College Partnership program in the summer of 2012, helped with some of the ice nucleation tests with *P. syringae*. Comments and suggestions from three anonymous reviewers are also appreciated.

APPENDIX

Dust Dispersal System

Aerosol is generated via a vibrating membrane upon which dust is placed. The membrane is enclosed and dry

HEPA-filtered air is pulled through the sealed volume. The lofted particles are then carried to the rest of the experiment. The vibrating membrane is driven by a 4-in. full-range audio speaker. A Wavetek 2-MHz function generator (model 20) drives the speaker with a 100-Hz sine wave amplified through a Memorex 2Xtreme radio circuit. The voltage output of the function generator determines the power of the speaker and subsequently the number concentration of the aerosol. Numbers from 10 to 1000 per cubic centimeter are readily achieved depending on the dust type. A schematic is shown in Fig. A1. The thin membrane is a heat shrinkable plastic available from Henkel Consumer Adhesives, Inc., as part of a window kit.

REFERENCES

- Bundke, U., B. Nillius, R. Jaenicke, T. Wetter, H. Klein, and H. Bingemer, 2008: The Fast Ice Nucleus Chamber FINCH. *Atmos. Res.*, **90**, 180–186, doi:10.1016/j.atmosres.2008.02.008.
- Finke, H., M. Gross, G. Waddington, and H. Huffman, 1954: Low-temperature thermal data for the nine normal paraffin hydrocarbons from octane to hexadecane. *J. Amer. Chem. Soc.*, **76**, 333–341, doi:10.1021/ja01631a005.
- Fletcher, A. N., 1972: High-temperature contact nucleation of supercooled water by organic chemicals. *J. Appl. Meteor.*, **11**, 988–993, doi:10.1175/1520-0450(1972)011<0988:HTCNOS>2.0.CO;2.
- Fornea, A., S. Brooks, J. Dooley, and A. Saha, 2009: Heterogeneous freezing of ice on atmospheric aerosols containing ash, soot, and soil. *J. Geophys. Res.*, **114**, D13201, doi:10.1029/2009JD011958.
- Gokhale, N., and J. Goold, Jr., 1968: Droplet freezing by surface nucleation. *J. Appl. Meteor.*, **7**, 870–874, doi:10.1175/1520-0450(1968)007<0870:DFBSN>2.0.CO;2.
- Hartmann, S., S. Augustin, T. Clauss, H. Wex, T. Šantl-Temkiv, J. Voigtländer, D. Niedermeier, and F. Stratmann, 2013: Immersion freezing of ice nucleation active protein complexes. *Atmos. Chem. Phys.*, **13**, 5751–5766, doi:10.5194/acp-13-5751-2013.
- Hoffmann, N., A. Kiselev, D. Rzesanke, D. Duft, and T. Leisner, 2013: Experimental quantification of contact freezing in an electrodynamic balance. *Atmos. Meas. Tech.*, **6**, 2373–2382, doi:10.5194/amt-6-2373-2013.
- Hussain, K., and C. P. R. Saunders, 1984: Ice nucleus measurement with a continuous flow chamber. *Quart. J. Roy. Meteor. Soc.*, **110**, 75–84, doi:10.1002/qj.49711046307.
- Ladino, L. A., O. Stetzer, F. Lüönd, A. Welti, and U. Lohmann, 2011: Contact freezing experiments of kaolinite particles with cloud droplets. *J. Geophys. Res.*, **116**, D22202, doi:10.1029/2011JD015727.
- , —, and U. Lohmann, 2013: Contact freezing: A review. *Atmos. Chem. Phys. Discuss.*, **13**, 7811–7869, doi:10.5194/acpd-13-7811-2013.
- López, M. L., and E. E. Ávila, 2013: Measurements of natural deposition ice nuclei in Crdoba, Argentina. *Atmos. Chem. Phys.*, **13**, 3111–3119, doi:10.5194/acp-13-3111-2013.
- Maki, L. R., E. L. Galyan, M.-M. Chang-Chien, and D. R. Caldwell, 1974: Ice nucleation induced by *Pseudomonas syringae*. *Appl. Microbiol.*, **28**, 456–459.

- Monier, J.-M., and S. E. Lindow, 2003: *Pseudomonas syringae* responds to the environment on leaves by cell size reduction. *Phytopathology*, **93**, 1209–1216, doi:10.1094/PHYTO.2003.93.10.1209.
- Pitter, R., and H. Pruppacher, 1973: A wind tunnel investigation of freezing of small water drops falling at terminal velocity in air. *Quart. J. Roy. Meteor. Soc.*, **99**, 540–550, doi:10.1002/qj.49709942111.
- Roberts, P., and J. Hallett, 1968: A laboratory study of the ice nucleating properties of some mineral dusts. *Quart. J. Roy. Meteor. Soc.*, **94**, 25–34, doi:10.1002/qj.49709439904.
- Rogers, D., 1988: Development of a continuous flow thermal gradient diffusion chamber for ice nucleation studies. *Atmos. Res.*, **22**, 149–181, doi:10.1016/0169-8095(88)90005-1.
- Shaw, R., A. Durant, and Y. Mi, 2005: Heterogeneous surface crystallization observed in undercooled water. *J. Phys. Chem.*, **109B**, 9865–9868, doi:10.1021/jp0506336.
- Svensson, E., C. Delval, P. von Hessberg, M. Johnson, and J. Pettersson, 2009: Freezing of water droplets colliding with kaolinite particles. *Atmos. Chem. Phys.*, **9**, 4295–4300, doi:10.5194/acp-9-4295-2009.
- Tomlinson, E. M., and N. Fukuta, 1985: A new horizontal gradient, continuous flow, ice thermal diffusion chamber. *J. Atmos. Oceanic Technol.*, **2**, 448–467, doi:10.1175/1520-0426(1985)002<0448:ANHGCF>2.0.CO;2.
- Yun, Y., and J. E. Penner, 2012: Global model comparison of heterogeneous ice nucleation parameterizations in mixed phase clouds. *J. Geophys. Res.*, **117**, D07203, doi:10.1029/2011JD016506.